

## Photoionized Herbig-Haro objects in the Orion Nebula through deep high-spectral resolution spectroscopy II: HH 204

J. E. MÉNDEZ-DELGADO,<sup>1,2</sup> C. ESTEBAN,<sup>1,2</sup> J. GARCÍA-ROJAS,<sup>1,2</sup> W. J. HENNEY,<sup>3</sup> A. MESA-DELGADO,<sup>4</sup> AND K. Z. ARELLANO-CÓRDOVA<sup>5</sup>

<sup>1</sup> Instituto de Astrofísica de Canarias (IAC), E-38205 La Laguna, Spain

<sup>2</sup> Departamento de Astrofísica, Universidad de La Laguna, E-38206 La Laguna, Spain

<sup>3</sup> Instituto de Radioastronomía y Astrofísica, Universidad Nacional Autónoma de México, Apartado Postal 3-72, 58090 Morelia, Michoacán, Mexico

<sup>4</sup> Calle Camino Real 64, Icod el Alto, Los Realejos, 38414, Tenerife, Spain

<sup>5</sup> The University of Texas at Austin, 2515 Speedway Boulevard Stop C1400, Austin, TX 78712, USA

(Received XXX; Revised YYY; Accepted ZZZ)

Submitted to ApJ

### ABSTRACT

Contribuciones de Will para el artículo

*Keywords:* ISM:Abundances – ISM: Herbig–Haro objects – ISM: individual: Orion Nebula – ISM: individual: HH 204

### 1. MATERIAL DE WILL

Pongo primero lo de *HST* porque es más completo.

#### 1.1. Sub-arcsecond imaging of HH 204

Figure 1a shows the ratio of surface brightnesses,  $R([\text{O III}]) = S([\text{O III}] \lambda 5007)/S(\text{H}\alpha \lambda 6563)$ , calculated from *HST* WFPC2 observations in the F502N, F547M, F656N, and F658N filters from program GO5469 (O’Dell & Wong 1996). Flux calibration and correction for contamination by continuum and non-target lines was performed using the coefficients given in O’Dell (2009). It can be seen that the line ratio in the background nebula shows a pronounced gradient from  $R([\text{O III}]) \approx 0.3$  in the north-east to  $R([\text{O III}]) \approx 0.5$  in the south-west.<sup>1</sup> Inside the bow shock, the ratio is significantly smaller, for instance falling from  $\approx 0.4$  to  $\approx 0.2$  along the length of the UVES slit.

However, the most interesting feature of the  $R([\text{O III}])$  image is the slight *increase* in the ratio that is seen in a

thin layer along the leading edge of the bow shock. This is most clearly visible in the northern wing of HH 204, such as the area highlighted by a dotted outline box in the figure. Average profiles across the shock for this region are shown in Figure 1b. The lower panel shows that the raw ratio (solid black line) increases only slightly above its value in the background nebula, which is because the brightness increase across the bow shock is only a small fraction of the background brightness, as can be appreciated in the upper panel. In order to isolate the emission of the shocked gas from that of the nebula, we calculate the background-subtracted line ratio:

$$R'([\text{O III}]) = \frac{S([\text{O III}]) - S_{\text{BG}}([\text{O III}])}{S(\text{H}\alpha) - S_{\text{BG}}(\text{H}\alpha)} \quad (1)$$

under the assumption that  $S_{\text{BG}}$  for each line is constant along the profile. The result is shown as a gray histogram in the lower panel of the figure, which reveals a sharp peak of width  $\approx 0.3$  mpc that reaches a maximum value  $R'([\text{O III}]) \approx 2R_{\text{BG}}([\text{O III}])$  and is centered on a displacement of  $\approx -0.1$  mpc. The origin of the displacement axis is set to the peak in the spatial gradient of the  $\text{H}\alpha$  surface brightness, corresponding to the outer edge of the dense shocked shell. The negative displacement of the  $R'([\text{O III}])$  peak means that this occurs *outside* the dense shell, closer to the shock front itself.

Corresponding author: José E. Méndez-Delgado  
 jemd@iac.es

<sup>1</sup> For comparison with results from our UVES spectra, and using the average reddening for the HH 204 region (Weillbacher et al. 2015), the conversion is  $\lambda 4959/\text{H}\beta \approx 1.1R([\text{O III}])$ .

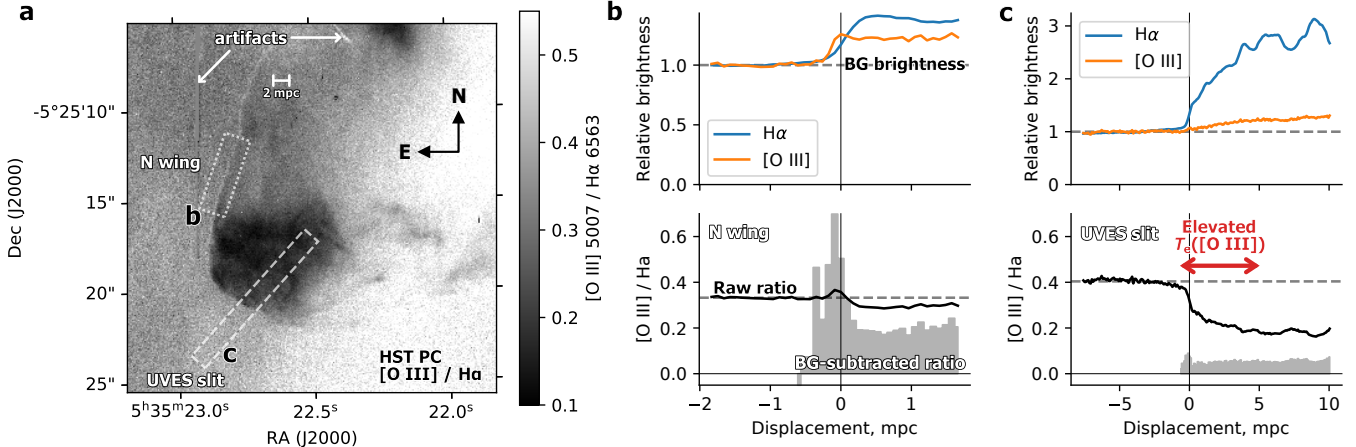


**Figure 1.** (a) Map of the line ratio  $[O\text{ III}]\lambda 5007/\text{H}\alpha\lambda 6563$ , calculated from *HST* images with the PC chip of the WFPC2 camera. The position of the UVES spectrograph slit is outlined by a dashed box, while a further region of interest in the N wing of the bow shock is indicated by a dotted box. The vertically oriented ‘scar’ at upper left is an artifact due to the bright star  $\theta^2$  Ori A, located just north of the field of view. (b) Average cut profiles of the *HST* images for the box in the N wing that is outlined in panel a. Upper graph shows surface brightness profiles in the two emission lines, normalized to the mean nebular background value outside of the shock. Lower graph shows the line ratio, with the raw ratio indicated by the black solid line and the background-subtracted ratio indicated by the gray histogram. The zero point of the displacement axis is taken to be the location of the maximum gradient in the  $\text{H}\alpha$  surface brightness. (c) Same as panel b, but showing average profiles of the *HST* images along the UVES slit. The region of the slit that shows  $T_e([O\text{ III}]) > 12\,000\text{ K}$  in the blueshifted component is indicated by the red arrow.

Figure 1c shows the same quantities calculated along a cut that coincides with our UVES slit at the head of HH 204. In this case,  $R'([O\text{ III}])$  is always significantly less than  $R_{\text{BG}}([O\text{ III}])$ , but it does still show a small local peak with a position and width that is similar to the more impressive one in the northern wing. These peaks in  $R'([O\text{ III}])$  occur over a much smaller scale than any of spatial gradients that we find in our UVES slit spectra and are only detectable because of the high spatial resolution of the *HST*.<sup>2</sup> For example, the increase in  $T_e([O\text{ III}])$  that we detect in the blue-shifted emission near the shock front (Figure 6) occurs over a scale of 5 mpc, indicated by the red arrow in the figure, which is more than 10 times larger than the width of the  $R'([O\text{ III}])$  peak.

#### Lo que sigue es más bien discusión

What is the origin of the narrow peak in the  $[O\text{ III}]/\text{H}\alpha$  ratio that is seen just outside the shocked shell? When a shock propagates into low-ionization gas (predominantly  $\text{O}^+$ ), there are three zones where enhanced  $[O\text{ III}]$  emission might be expected (Cox & Raymond 1985; Sutherland & Dopita 2017): first, the radiative precursor in the pre-shock gas; second, the non-equilibrium collisional ionization zone immediately after the shock; third, the radiative relaxation zone where the post-shock gas cools

back down to the photoionization equilibrium temperature of  $\sim 10^4\text{ K}$ . The first of these can be ruled out in the case of HH 204 because the pre-shock photoionization of  $\text{O}^+$  would require shock velocities greater than  $150\text{ km s}^{-1}$ . (*Check the exact number. All the shock papers only give the velocity to pre-ionize hydrogen.*) The second zone has a high temperature ( $> 50\,000\text{ K}$  for shock velocities  $> 55\text{ km s}^{-1}$ ) but is severely underionized, resulting in line emissivities that are far in excess of the equilibrium values. However, the region that can emit  $[O\text{ III}]$  lines is likely to be extremely thin due to the high collisional ionization rate (*make an estimate of the thickness*). The third zone, in which oxygen is recombining through the  $\text{O}^{++}$  stage while cooling through the range  $20\,000\text{ K}$  to  $10\,000\text{ K}$ , is therefore the most promising origin.

*Calculate the cooling length and show that in the wings, where the post-shock density is less than  $10^4\text{ cm}^{-3}$ , we should resolve the cooling zone, whereas at the bow shock head where the density is greater than  $2 \times 10^4\text{ cm}^{-3}$ , it will be unresolved. This may explain why we only clearly see the peak in  $R'([O\text{ III}])$  in the wing. (But this may also be due to dilution by the Mach disk, see below).*

*Then, how to explain the behavior of  $T_e([O\text{ III}])$ , which varies on much larger scales than the cooling length. Possibly related to the radius of curvature of the shock. Alternatively, could be that we are seeing a mixture of*

<sup>2</sup> Pixel size of 0.045 arcsec, which well samples the PSF width at  $\text{H}\alpha$  of 0.083 arcsec.

*the two shocked shells: the one from behind the bow shock and the one from behind the Mach disk (jet shock). As we move along the slit away from the shock, the Mach disk shell dominates more and more. If the jet shock is lower velocity than the bow shock, then this might explain the observed gradient in the [O III] temperature. This is also consistent with the appearance of the object: there is a big clump of emission that disappears once you move away from the axis into the wings, while the bow shock part remains.*

### 1.2. Origin of the jet that drives HH 204

At least two different high-velocity flows converge on the general HH 203/204 region from the direction of the inner Orion Nebula (see Figure 2), but it is not clear if either of them are directly responsible for driving the HH 204 bow shock. One flow is at a position angle (PA) of  $\approx 118^\circ$  and transitions from a high ionization state north-west of the Bright Bar (cyan contours in Fig. 2a), to a lower ionization state (yellow contours) to the south-east of the Bright Bar. The other is at PA  $\approx 140^\circ$  and is of low ionization for its entire detected length. Both these flows give the appearance of driving HH 203, which implies that HH 203 may be a superposition of two unrelated bow shocks. Such a superposition is consistent with the detection of two different velocity components ( $-73$  and  $-39 \text{ km s}^{-1}$ ) at the head of the bow shock, and also with the complex structure apparent in high-resolution *HST* images (see Fig. 2b). O'Dell et al. (2015) noted that in addition to the main bow shock (HH 203a), there appears to be a second faint bow shock (HH 203b), associated with the PA118 flow. We also detect a third faint bow shock, which we denote HH 203c, situated in front (SW) of HH 204a. Note that O'Dell et al. (2015) give position angles of  $124^\circ$  and  $127^\circ$ , respectively, for HH 203 and HH 204, which

probably represent an average of the PA118 and PA140 flows.

The southern portion of HH 203a, which we label as “[S II] knot” in the figure, is particularly strong in the [S II] and [O I] filters and coincides with the peak of the  $-39 \text{ km s}^{-1}$  feature. The spatial alignment and the similarity in velocity and ionization makes it likely that this knot is part of the PA140 flow. It is conceivable that this flow may extend farther to the SW and be driving the HH 204 bow shock, although there is no direct evidence for this. On the other hand, a third flow at PA  $\approx 108^\circ$  is seen to feed into HH 204 from the west. This jet, first noted by Doi et al. (2004), is very short and stubby, and can be traced back only 10 arcsec (20 mpc) from the bow shock. There is another faint filament of high-velocity [O III] emission that extends between the HH 203 and HH 204 regions at PA  $\approx 108^\circ$  (see Fig. 2a). This appears to provide a connecting bridge between the PA140 and PA108 flows, although the difference in velocity and ionization with respect to the PA108 flow argues against a physical association with HH 204.

In summary, convincing evidence for which large scale flow might be driving the HH 204 bow shock is frustratingly absent. Although the PA108 flow is clearly associated with HH 204, its short length means that the exact orientation is very uncertain. The PA140 flow has a much better defined direction, but its extension beyond the position of the [S II] knot in order to feed into the HH 204 bow shock is purely speculative. The only thing that can be said with any degree of certainty is that the high-ionization PA118 flow is *not* driving HH 204, but only HH 203. In Figure 2b we show the back projection of all three of these flows into the core of the nebula, assuming an uncertainty of  $\pm 10^\circ$  for the PA108 flow and  $\pm 5^\circ$  for the other two.

## REFERENCES

- Cox, D. P., & Raymond, J. C. 1985, ApJ, 298, 651  
 Doi, T., O'Dell, C. R., & Hartigan, P. 2004, AJ, 127, 3456  
 García-Díaz, M. T., Henney, W. J., López, J. A., & Doi, T. 2008, RMxAA, 44, 181  
 O'Dell, C. R. 2009, PASP, 121, 428  
 O'Dell, C. R., Ferland, G. J., Henney, W. J., et al. 2015, AJ, 150, 108  
 O'Dell, C. R., & Wong, K. 1996, AJ, 111, 846  
 Sutherland, R. S., & Dopita, M. A. 2017, ApJS, 229, 34  
 Weilbacher, P. M., Monreal-Ibero, A., Kollatschny, W., et al. 2015, A&A, 582, A114

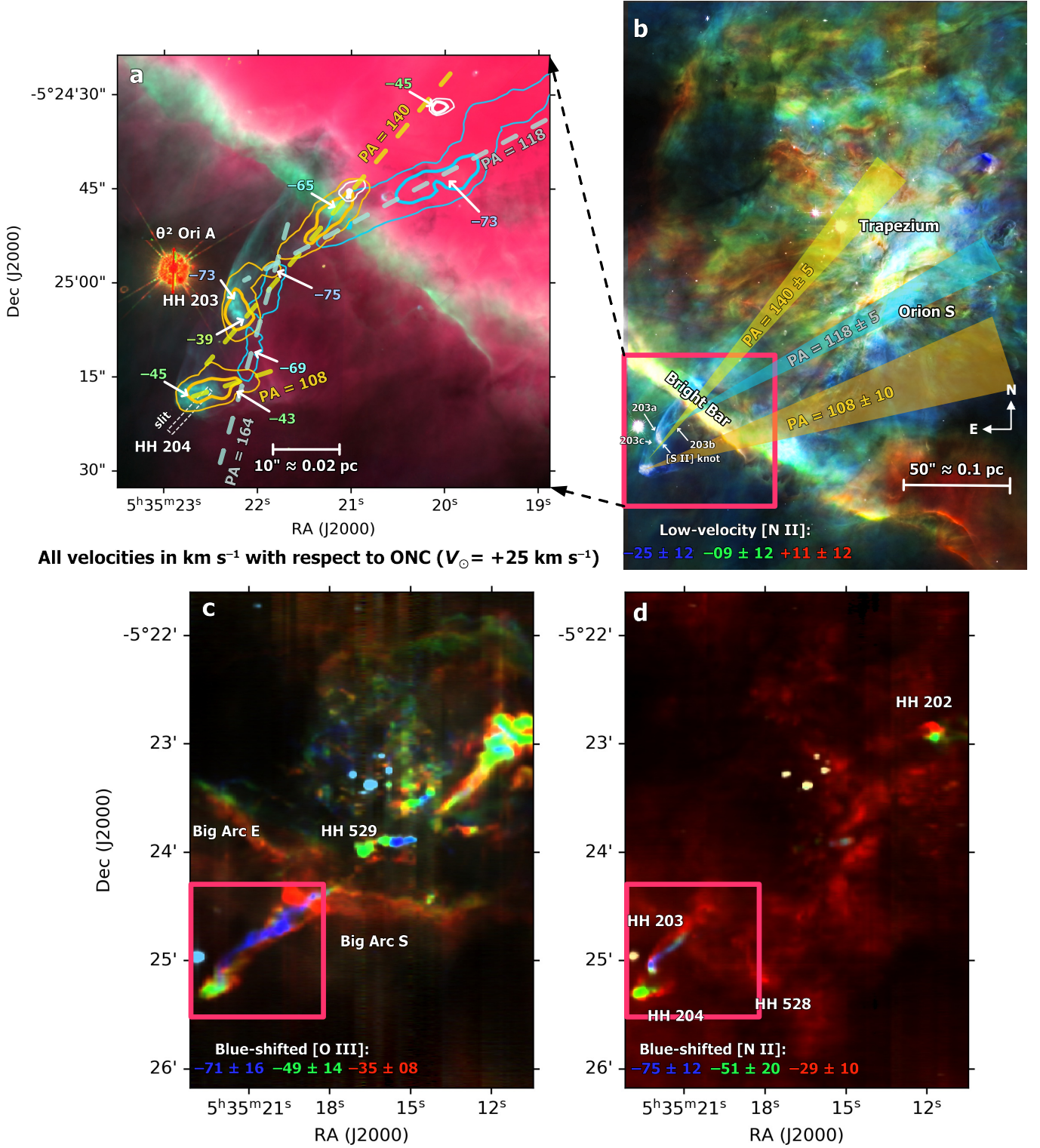


**Figure 2.** Location of HH 204 within the Orion Nebula. (a) Position of the UVES slit for our spectroscopic observations (white dashed box), shown superimposed on an RGB emission-line image of the environs of HH 203 and 204, derived from *HST* WFPC2 observations (O'Dell & Wong 1996) in filters of [O III] (red), [N II] (green), and H $\alpha$  (blue). Contours show highly blue-shifted emission of [O III] (cyan, centered on  $-70 \text{ km s}^{-1}$ ) and [N II] (yellow, centered on  $-50 \text{ km s}^{-1}$ , and white, centered on  $-35 \text{ km s}^{-1}$ ), derived from multiple longslit spectra (Doi et al. 2004 as recalibrated in spectral atlas of García-Díaz et al. 2008). Mean velocities with respect to the Orion Nebular Cluster of particular features related to the HH objects are indicated by arrows. (b) Location of HH 204 with respect to the inner Orion Nebula. The intensity of the image comes from the [N II] *HST* WFPC2 observations, but colorized according to the velocity of the slow-moving nebular gas (within about  $30 \text{ km s}^{-1}$  of the systemic velocity) as derived from the longslit spectra, see color key on figure. (c) Highly blue-shifted [O III] emission for a field of view similar to that of panel b. (d) As panel c but for highly blue-shifted [N II] emission.